Season-dependent weather predictability barrier phenomenon in the Martian atmosphere

Yi Zhuang *(1,2)*, **Wansuo Duan** *(1,2; duanws@lasg.iap.ac.cn)*, **Li Dong** *(1,2)*
(1) Institute of Atmospheric Physics, Chinese Academy of Sciences, Beijing, China
(2) University of Chinese Academy of Sciences, Beijing, China

Introduction:

In contemporary deep space exploration, Mars has emerged as a prime target, owing to its proximity and Earth-like qualities. Currently, Martian rovers are the most advanced technology for Mars exploration, and are expected to play an important role in future Mars missions. However, the severe conditions of the Martian atmosphere pose great challenges to the Martian rovers, making accurate Martian weather forecast a dominant research objective.

Even though the Martian atmosphere shares much similarities with Earth atmosphere[1,2], its predictability might be poles apart from common senses on Earth. Since Lorenz's work in the 1960s, scientists have come to recognize that for Earth atmosphere, small initial errors will grow fast and there exists two-week predictability limit for weather forecasts[3–9]. Nevertheless, there has not yet been a consensus reached on Martian atmosphere predictability. Newmann et al. showed that the Martian atmosphere is remarkably predictable during Northern Hemisphere summer, and the errors only grow rapidly in winter[10], but some other studies argued that positive error growth rate persists through most time of the year[11,12]. Clearly, the predictability limit of Martian atmosphere remains open to discussion, and there is an urgent need to reveal more valuable insights on the predictability of Martian atmosphere.

Here, we disclose a season-dependent weather predictability barrier (S-WPB) phenomenon in Martian atmosphere by applying the bred vector (BV) method, where the BVs represent the unstable modes in the Martian atmosphere[5,6,10,13]. The S-WPB is referred to as a phenomenon that initial temperature errors are most likely to exhibit significant growth when performing weather forecast experiments during particular seasons.

In this study, the LMD Mars PCM model is used. This model reasonably reproduces realistic Martian atmospheric fields including temperature, wind and water cycles, etc., and has been extensively applied in Martian atmosphere research over the past decades[14–19]. Furthermore, this S-WPB is also indicated by the Ensemble Mars Atmosphere Reanalysis System (EMARS) reanalysis data[20] (See Figure 1). It is therefore quite plausible that the S-WPB phenomenon will occur in realistic predictions of Martian atmosphere, though currently no operational Martian weather forecasting system produces publicly available prediction data.

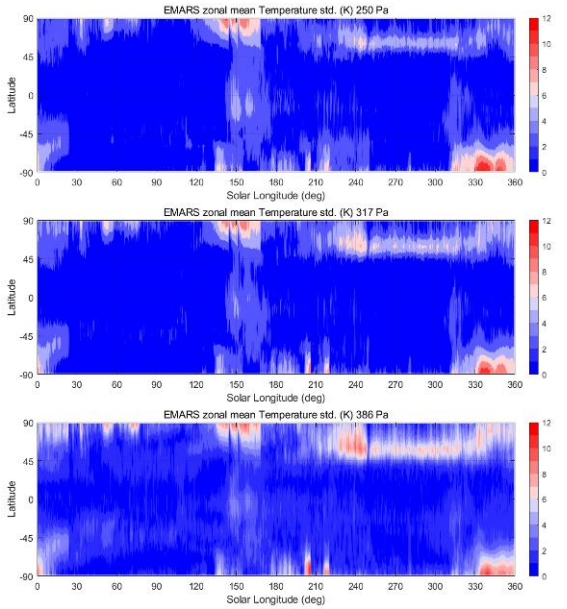

Figure 1: Spatiotemporal variability of EMARS temperature standard deviation across different pressure levels. Based on EMARS v1.0 reanalysis, zonal mean temperature standard deviations across MY 26 and MY 29-32 are computed (excluding global dust storm years and years with limited observations from MY 25 to MY 32). The pressure levels are labeled above each panel.

Methods For Quantifying Predictability:

Error size and growth rate. In current study, the size of errors (both for initial errors and forecast errors) is measured by the global temperature RMSE, weighted by the grid air mass. The size of initial errors is selected as 1 K. As the growing of small error in short period is assumed to follow exponential rule[10–12], the error growth rate can be calculated as the logarithm of the ratio of the forecast error size to the initial error size.

Bred vector method. The bred vector method is proposed to identify the growing error mode in atmospheric models[5,6]. It is centered on the idea that the errors will grow in the unstable direction while shrink in the stable direction, and hence the fast-growing mode is developed through this breeding procedure. The diagram shown in Figure 2 illustrates how bred vector is obtained through the forecast-rescaling cycles in current study, focusing on the initial error growth.

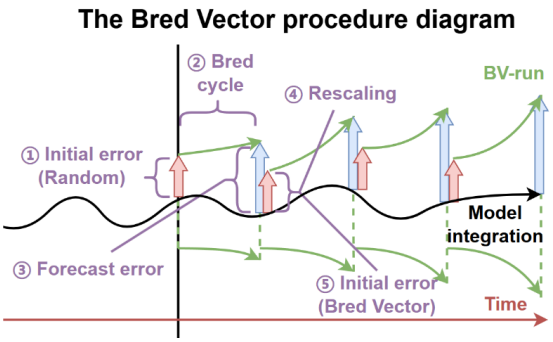

Figure 2: The bred vector procedure diagram. At the beginning of the procedure, randomly generated initial errors are superimposed on the initial field. After integrating for a bred cycle, the forecast error size is calculated and the error is scaled back to the original size, which is then superimposed on initial fields at next step for the next cycle.

The S-WPB Phenomenon:

The time series of the global Martian atmospheric temperature field are obtained through integrating the model initialized from the available Martian Climate Database (MCD) restart data on equinoxes and solstices across MY 25 to MY 32 with realistic dust scenario forcing[14,21,22]. These time series are treated as the reference states to be forecasted, while our weather forecast experiments are done by imposing initial temperature errors on these reference states and then integrating the model forwards.

As Figure 3 shows, larger positive error growth occurs when the initial errors characterized by BVs are imposed during both late summer and early spring, indicating that the Martian atmospheric temperature forecasts tend to undergo both summer-WPB and spring-WPB. Further investigation reveals that the WPB occurrence particularly depends on specific season, geographical location and specific initial error pattern, while randomly generated errors lack these characteristics and fails to grow.

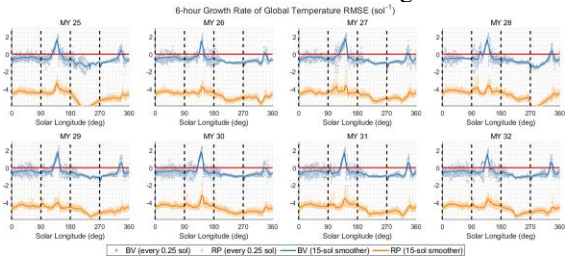

Figure 3: The growth rate of the errors derived by BVs and RPs for the forecasts of global temperatures from MY 25 to MY 32. The growth rate is calculated from the Root-Mean-Square Error (RMSE) of the global temperature field. Blue dots represent the growth rate of BV errors spanning a time interval of 6 Martian hours or 0.25 sol, while orange dots denote those of RP errors during the same time interval. The blue and orange lines are respectively derived by applying a 15-sol average, highlighting the seasonal variation features. The vertical black dashed lines mark the equinoxes and solstices when model integration initializes with MCD restart data as well as when breeding procedure starts. Horizontal thick red line serves as a reference of zero value.

The Environmental Condition For S-WPB:

In-depth diagnosis reveals that the error growth is sensitive to the saturated water vapor in polar regions, where water ice-radiation feedback takes effect. To quantify this environmental condition, we propose a novel "condensation potential" index to quantify the amount of water ice that condenses if the atmosphere encounters certain extent of cooling. Figure 4 illustrates the spatiotemporal distribution of the condensation potential index and relevant fields, using MY 25 as a representative year. It is clear that large condensation potential occurs in late summer and early spring, the same season as WPB.

Other season and geographical locations that not undergo WPB generally possess little condensation potential. For these cases, two distinct atmospheric regimes are identified. The first kind typically occurs in warm regions and seasons. For this kind of state, the water vapor is sufficient, but the temperature is rather warm, resulting in low saturation ratio and little water vapor condenses when cooling occurs. The second kind typically occurs in cold regions and seasons, where the saturation ratio is usually high but the total amount of water vapor that can condense is deficient. Furthermore, the seasonal asymmetry of S-WPB phenomenon, as spring-WPB is shorter and weaker compared to the summer-WPB, can be explained by the much warmer atmosphere when Mars is around the perihelion.

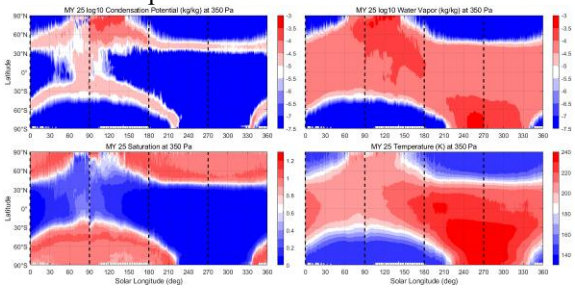

Figure 4: The spatiotemporal distribution of the condensation potential index and corresponding fields in the reference state as a function of latitude and solar longitude. MY 25 zonally averaged fields at 350 Pa are shown as representative examples. The dotted area around the South Pole marks corresponding topography where surface pressure is below 350 Pa. From left to right and top to bottom: condensation potential, water vapor, water vapor saturation ratio, temperature.

Discussion:

The radiative effect of water ice cloud in the Martian atmosphere has been prioritized in recent studies[16,23–25], and our study confirms that despite its low abundance, water vapor exerts a significant radiative effect on the Martian atmospheric predictability, in terms of temperature. It is also certainly noted that for bringing the temperature simulation closer to real Martian atmosphere, the model used in present study keeps dust distribution prescribed by realistic data, and does not describe the feedback between dust, water and atmospheric motion. Certainly, it is expected that future studies adopting models with fully

interactive dust scheme may reveal dust-related instabilities both during dust storm seasons and in relevant locations[2,26].

In any case, given the limited spatiotemporal coverage of Martian atmospheric observations, current Martian atmospheric models remain the first approximation, which provides valuable insights of Martian atmospheric predictability. On account of the S-WPB phenomenon, for the smooth running of affected Mars exploration missions in future, further measures like targeted observation are required to address the negative impacts of the S-WPB phenomenon. Moreover, as water and atmosphere are the primary conditions for the existence of life, similar phenomenon may also be widely present on various habitable terrestrial planets throughout the universe. Hence, uncovering the mystery of the Martian atmospheric predictability also enhances our understanding about potential weather predictability characteristics on habitable planets.

Future Work:

While BVs represent unstable modes from past data, their ability to represent future forecasting uncertainties is limited. To tackle this problem, we employ the conditional nonlinear optimal perturbation (CNOP) method proposed by Mu et al. in 2003[27]. The CNOP represents the initial error that causes maximum forecast error, and is obtained through solving a nonlinear optimization problem. Consider the following equations which outline the evolution of the atmospheric system:

$$\partial_t U = F(U(x,t)),\ U(t=0) = u_0,$$

where U represents atmospheric variables like temperature, wind and tracers. This system defines a unique evolution trajectory starting from the initial state u_0 to the forecast state u_T at time T, which can be denoted formally with the nonlinear propagator M:

$$M_T(u_0) = u_T.$$

Our aim is to find the optimal initial error δu_0 which induces largest forecast error δu_T at time T, but the initial error must be constrained in size for it to remain relevant to practical forecasting. Hence, the optimization problem can be described as follows:

$$\delta u_0 = \arg\max\{||M_T(u_0+\delta u_0) - M_T(u_0)||;\ ||\delta u_0|| \leqslant \delta_0\}.$$

Traditionally, this optimization problem is solved numerically by the combination of an adjoint model and optimization algorithms. The former provides gradient while the latter searches for the optimum. Since the LMD Mars PCM lacks an adjoint model currently, we propose an experience-guided-basis spectral projected gradient (EGB-SPG) for the CNOP calculation, which contains a "self-learning" module that can acquire knowledge comprehensively from historical optimization results via SPG optimization algorithms[28], achieving reasonable results with minimal computational cost. It is expected that the CNOP approach will uncover more valuable insights for the predictability of the Martian atmosphere.

Reference:

1. Lewis, S. R. Modelling the martian atmosphere. *Astron. Geophys.* **44**, 4.06-4.14 (2003).
2. Wu, Z. *et al.* Earth-like thermal and dynamical coupling processes in the Martian climate system. *Earth-Sci. Rev.* **229**, 104023 (2022).
3. Lorenz, E. N. The predictability of a flow which possesses many scales of motion. *Tellus* **21**, 289–307 (1969).
4. Lorenz, E. N. Atmospheric predictability experiments with a large numerical model. *Tellus* **34**, 505–513 (1982).
5. Toth, Z. & Kalnay, E. Ensemble Forecasting at NMC: The Generation of Perturbations. *Bull. Am. Meteorol. Soc.* **74**, 2317–2330 (1993).
6. Toth, Z. & Kalnay, E. Ensemble Forecasting at NCEP and the Breeding Method. *Mon. Weather Rev.* **125**, 3297–3319 (1997).
7. Palmer, T. N., Gelaro, R., Barkmeijer, J. & Buizza, R. Singular Vectors, Metrics, and Adaptive Observations. *J. Atmospheric Sci.* **55**, 633–653 (1998).
8. Mu, M., Wansuo, D. & Jifan, C. Recent advances in predictability studies in China (1999–2002). *Adv. Atmospheric Sci.* **21**, 437–443 (2004).
9. Duan, W. *et al.* Recent Advances in China on the Predictability of Weather and Climate. *Adv. Atmospheric Sci.* **40**, 1521–1547 (2023).
10. Newman, C. E., Read, P. L. & Lewis, S. R. Investigating atmospheric predictability on Mars using breeding vectors in a general-circulation model. *Q. J. R. Meteorol. Soc.* **130**, 2971–2989 (2004).
11. Rogberg, P., Read, P. L., Lewis, S. R. & Montabone, L. Assessing atmospheric predictability on Mars using numerical weather prediction and data assimilation. *Q. J. R. Meteorol. Soc.* **136**, 1614–1635 (2010).
12. Greybush, S. J., Kalnay, E., Hoffman, M. J. & Wilson, R. J. Identifying Martian atmospheric instabilities and their physical origins using bred vectors. *Q. J. R. Meteorol. Soc.* **139**, 639–653 (2013).
13. Corazza, M. *et al.* Use of the breeding technique to estimate the structure of the analysis 'errors of the day'. *Nonlin Process. Geophys* **10**, 233–243 (2003).
14. Forget, F. *et al.* Improved general circulation models of the Martian atmosphere from the surface to above 80 km. *J. Geophys. Res. Planets* **104**, 24155–24175 (1999).
15. Montmessin, F., Forget, F., Rannou, P., Cabane, M. & Haberle, R. M. Origin and role of water ice clouds in the Martian water cycle as inferred from a general circulation model. *J. Geophys. Res. Planets* **109**, (2004).
16. Madeleine, J.-B., Forget, F., Millour, E., Navarro, T. & Spiga, A. The influence of radiatively active water ice clouds on the Martian climate.

Geophys. Res. Lett. **39**, (2012).
17. Navarro, T. *et al.* The Challenge of Atmospheric Data Assimilation on Mars. *Earth Space Sci.* **4**, 690–722 (2017).
18. Pottier, A. *et al.* Unraveling the martian water cycle with high-resolution global climate simulations. *Icarus* **291**, 82–106 (2017).
19. Connour, K. *et al.* Inferences of water–ice cloud physics determined from MAVEN/IUVS aerosol retrievals and Mars GCM comparisons. *Icarus* **421**, 116228 (2024).
20. Greybush, S. J. *et al.* The Ensemble Mars Atmosphere Reanalysis System (EMARS) Version 1.0. *Geosci. Data J.* **6**, 137–150 (2019).
21. Montabone, L. *et al.* Eight-year climatology of dust optical depth on Mars. *Icarus* **251**, 65–95 (2015).
22. Millour, E. *et al.* The Mars Climate Database (Version 6.1). in EPSC2022-786 (2022). doi:10.5194/epsc2022-786.
23. Urata, R. A. & Toon, O. B. Simulations of the martian hydrologic cycle with a general circulation model: Implications for the ancient martian climate. *Icarus* **226**, 229–250 (2013).
24. Navarro, T. *et al.* Global climate modeling of the Martian water cycle with improved microphysics and radiatively active water ice clouds. *J. Geophys. Res. Planets* **119**, 1479–1495 (2014).
25. Chow, K. C. Simulation of the Martian Water Cycle with a Coupled Interactive Dust Cycle. in vol. 3007 3322 (2024).
26. Rafkin, S. C. R. A positive radiative-dynamic feedback mechanism for the maintenance and growth of Martian dust storms. *J. Geophys. Res. Planets* **114**, (2009).
27. Mu, M., Duan, W. S. & Wang, B. Conditional nonlinear optimal perturbation and its applications. *Nonlinear Process. Geophys.* **10**, 493–501 (2003).
28. Birgin, E. G., Martínez, J. M. & Raydan, M. Nonmonotone Spectral Projected Gradient Methods on Convex Sets. *SIAM J. Optim.* **10**, 1196–1211 (2000).